Angewandte Chemie International Edition

Angewandte International Edition Chemie

How to cite: *Angew. Chem. Int. Ed.* **2026**, 65, e2431054
doi.org/10.1002/anie.2431054

RESEARCH ARTICLE OPEN ACCESS

Facet-Dependent Water Inhibition of Alkanol Dehydration on TiO_2 via Distinct Water–Alkanol Complexes

Wenda Hu[1,2] | Haiting Cai[2] | Anthony Savoy[1] | Jinshu Tian[3] | Sungmin Kim[2] | Fan Lin[2] | Junrui Li[1] | Hao Xu[1] | Yiqing Wu[2] | Zihao Zhang[4] | Nicholas Jaegers[1,2] | Huamin Wang[2] | Feng Gao[2] | Jianzhi Hu[1,2] | Yong Wang[1,2]

[1]The Gene and Linda Voiland School of Chemical Engineering and Bioengineering, Washington State University, Pullman, Washington, USA | [2]Institute for Integrated Catalysis, Pacific Northwest National Laboratory, Richland, Washington, USA | [3]Zhejiang Key Laboratory of Surface and Interface Science and Engineering for Catalysts, College of Chemical Engineering, Zhejiang University of Technology, Hangzhou, Zhejiang, China | [4]Center for Renewable Carbon, School of Natural Resources, University of Tennessee, Knoxville, Tennessee, USA

Correspondence: Feng Gao (feng_fgao@tju.edu.cn) | Jianzhi Hu (jianzhi.hu@pnnl.gov) | Yong Wang (yong.wang@pnnl.gov)

Received: 5 March 2026 | **Revised:** 19 May 2026 | **Accepted:** 22 May 2026

Keywords: alkanol dehydration | facet-dependent | TiO_2 facet | water effect

ABSTRACT

Water is ubiquitous in biomass-derived feeds, yet its molecular impact on oxygen-elimination reactions remains poorly understood, particularly for catalysts exposing different facets. Here, we utilize well-defined TiO_2 nanocrystals with dominant (101) and (001) facets to reveal a pronounced facet-dependent effect of water, where inhibition for dehydration of isopropanol (IPA) on the TiO_2(001) surface is about four times more severe than TiO_2(101). Through a combination of in situ solid state NMR, in situ infrared spectroscopy, kinetics studies, and theoretical calculations, we demonstrate that this disparity arises from the formation of distinct alkanol-water complex intermediates. On TiO_2(001), IPA undergoes dissociative adsorption to form an isopropoxide-H_2O complex that readily drives the surface into a complex-dominated regime. This pathway increases the activation barrier for C–H cleavage by 40 kJ mol^{-1} by inducing a disordered transition state. In contrast, TiO_2(101) favors molecular IPA adsorption with weak hydrogen bonding to water, resulting in a smaller complex formation constant and a much smaller activation barrier increase (25 kJ mol^{-1}). By quantitatively linking facet-dependent complex coverage to transition-state destabilization, this work moves beyond simple site-blocking models and provides a conceptual framework for designing catalysts that remain active in water-containing environments.

1 | Introduction

Biomass upgrading is critical for producing renewable chemicals and fuels [1–4]. Among various deoxygenation strategies, catalytic dehydration of biomass-derived alcohols, polyols, and cycloalkanols is widely employed. Representative examples include fructose dehydration to hydroxymethylfurfural [5], dehydration of glycerol [6], and propene production from propanol [7]. However, a major challenge in these processes is the ubiquitous presence of water. Biomass feedstocks typically contain 6–95% water [8], and dehydration reactions inherently generate water as a product. Consequently, understanding how water influences alcohol dehydration is both fundamentally important and practically relevant for biomass conversion.

Water is widely recognized as a potent modulator of catalytic reactivity. In many oxide-catalyzed systems, water often suppresses activity or accelerates deactivation [9, 10], although it can

Wenda Hu and Haiting Cai contributed equally to this work.

also enhance reactivity in specific systems such as alkane C–H activation [11], H–D exchange [12], and acid sites activation [13]. Mechanistically, water has been proposed to influence reactions through competitive adsorption, intermediate stabilization, or by forming unreactive species [14, 15]. Roy et al. [16] discovered that in ethanol and propanol dehydration on γ-Al_2O_3, water competes for surface sites without altering activation barriers but adsorbs strongly enough to suppress alcohol adsorption. Zhi et al. [17] studied dehydration pathways of propanol on ZSM-5 zeolites in the presence and absence of water and discovered an increase of activation barrier by forming a water-propanol complex. Lin et al. [18] reported that the formation of bridging bidentate carboxylate associated with H_2O leads to a higher ketonization activation barrier on TiO_2. The formation of unreactive complexes, such as ethanol-water heterodimers, was also observed in alcohol dehydration on Keggin-type polyoxometalate clusters, γ-Al_2O_3, and TiO_2 [19–22]. On Nb_2O_5, water dissociation generates Brønsted acid sites and decreases Lewis acidity, altering catalytic behavior [23]. In zeolites, Brønsted acid sites are solvated by water to form hydronium ions (H_3O^+), as shown by solid-state NMR [24]. Bates et al. [25] revealed stabilization of $(C_2H_5OH)(H_3O^+)(H_2O)_{4–5}$ clusters in zeolite pores, which lowers the dehydration rate by decreasing the reaction order of ethanol.

Despite these insights, the molecular origins of water-induced inhibition on heterogeneous oxide catalysts remain poorly understood. This gap arises from the lack of direct molecular-level experimental evidence, and this elucidation is especially challenging because catalysts, for example, TiO_2, expose multiple facets with distinct adsorption geometries and acid–base properties. TiO_2 facets, such as the (101), (001), and (100) surfaces, exhibit markedly different surface energies (0.44, 0.90, and 0.53 J m^{-2}, respectively) [26], leading to facet-dependent reactivities in methanol decomposition, alkanol dehydration, and aldol condensation [27–34]. Water–surface interactions also vary by facet: molecular water adsorbs preferentially on TiO_2(101), while TiO_2(001) favors dissociative adsorption at low coverages [35]. Therefore, these contrasts suggest that water may not affect dehydration uniformly across facets but rather interact with adsorbates in fundamentally different ways depending on the surface atomic arrangement. Recent advances have enabled facet engineering to expose well-defined TiO_2 facets, thereby reducing surface heterogeneity and offering a powerful platform to probe structure–reactivity relationships [36–38]. Despite this opportunity, a molecular-level understanding of facet-specific water effects under reaction-relevant conditions is lacking. Most prior studies rely on either ultra-high-vacuum surface science or microscopic kinetic analysis, without directly correlating facet-dependent adsorption structures to measured activation parameters. In particular, it remains unclear whether water simply reduces the number of available active sites or instead modifies the geometry, binding strength, and transition state through specific hydrogen-bonding interactions with surface intermediates [17, 35, 39].

In this study, we address this question by systematically investigating how water modulates IPA dehydration on anatase TiO_2 with (101) and (001) dominant facets, respectively, to unravel two distinct facet-dependent water inhibition mechanisms at a molecular level. Compared to multifunctional substrates such as glycerol or sugars, which may undergo parallel reactions (e.g., rearrangement, C–C cleavage, oligomerization) that obscure surface chemistry, isopropanol (IPA) with a simple structure allows for direct probing of adsorption configurations, surface intermediates, and their interaction with co-adsorbed water. Furthermore, as a well-defined reaction involving the removal of one hydroxyl group and one H atom, using IPA dehydration as a probe reaction enables a clear and unambiguous investigation of how water influences reaction intermediates and activation energies on specific TiO_2 facets. With a combination of transient and steady-state reaction kinetics, including isotope labeling, in situ ^1H-^{13}C cross polarization (CP) and direct polarization (DP) magic angle spinning (MAS) NMR, in situ IR spectroscopies, and density functional theory (DFT) calculations, we demonstrate that water inhibition is fundamentally facet-dependent and not due to competitive adsorption. Instead, water reorganizes the adsorbate through the formation of distinct alcohol–water complexes depending on the underlying facet. On TiO_2(001), water interacts strongly with dissociatively adsorbed isopropoxide to form a hydrogen-bonded isopropoxide–H_2O complex dominating on the surface that significantly perturbs adsorption geometry and increases the activation barrier for E2 elimination. In contrast, on TiO_2(101), water interacts more weakly with molecularly adsorbed IPA, leading to a smaller complex formation constant and a more modest increase in activation barrier. This work establishes that water inhibition on oxide catalysts arises from facet-specific solvation of surface intermediates. Beyond IPA dehydration, the resulting insights into facet-dependent adsorption modes, hydrogen-bonding environments, and associated enthalpic penalties reflect general principles governing alcohol dehydration under water-containing conditions. These findings advance conventional site-blocking descriptions and highlight the importance of facet control in dictating how interfacial hydrogen-bond networks reshape catalysis under water-rich conditions.

2 | Results and Discussion

2.1 | Physicochemical Properties of the Model Catalysts

TiO_2(101) and (001) samples prepared by the two-step hydrothermal synthesis exhibit distinct physicochemical properties [31–33, 40–43]. The XRD patterns shown in Figure S1 demonstrate the anatase phase of synthesized TiO_2(101) and (001). Figure 1A,B shows transmission electron microscopy (TEM) and scanning electron microscopy (SEM) images of the TiO_2(001) sample, which exhibits a nanosheet morphology with an average lateral dimension of ~300 nm. Facet analysis indicates ~60% exposure of (001) facets (highlighted in blue in the inset model), with the remainder predominantly (101) facets (green), detailed in Supporting Information: Note 2, Figure S2, and Table S1. The sample has a surface area of 11 m^2 g^{-1}. Figure 1C,D presents TEM and SEM images of the TiO_2(101) sample, displaying a bipyramidal morphology with an average particle size of ~200 nm. Shape analysis reveals ~93% exposure of (101) facets, with minor (001) contributions, mainly at particle tips. This sample exhibits a surface area of 17 m^2 g^{-1}. Post-reaction analysis confirms that both the morphology and the relative (001)/(101) facet ratios are preserved within experimental uncertainty, indicating that the exposed TiO_2 surfaces remain stable under reaction conditions

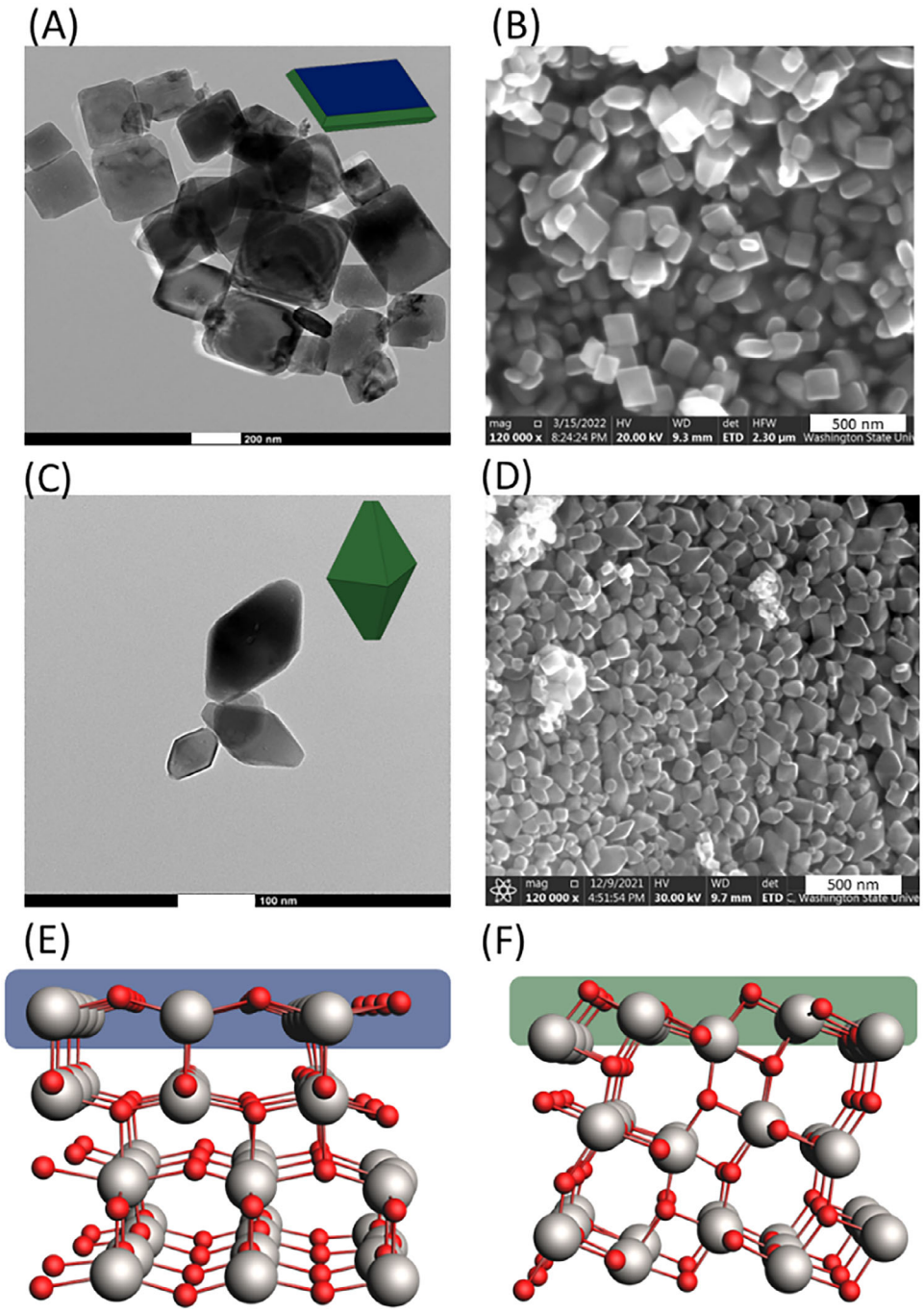

FIGURE 1 | (A) and (B) TEM and SEM images of the TiO_2(001); (C) and (D) TEM and SEM images of the TiO_2(101); ball and stick models of (E) (001) and (F) (101).

(Figure S2C,D). Ball-and-stick models of the TiO_2 surfaces are shown in Figure 1E,F. The (001) surface exhibits a relatively flat atomic arrangement, whereas the (101) surface displays a corrugated arrangement with alternating rows of Ti and O atoms. Densities of surface Lewis acid sites were determined by NH_3-temperature programed desorption (TPD). As shown in Figure S3A, NH_3 desorbs at a relatively higher temperature from TiO_2(001) than (101), consistent with a previous report [31]. The Lewis acid site density was calculated from NH_3 uptake, yielding 21 and 14 µmol g^{-1} for TiO_2(101) and (001), respectively, and was used for turnover frequency (TOF) normalization (Supporting Information, experimental section).

2.2 | Kinetic Performance of Facet-Dependent Water Impact on IPA Dehydration

Figure 2 presents the kinetic dependences of steady-state IPA dehydration on TiO_2(101) and (001) at 250–280°C and an ambient pressure with 0.25–8 kPa IPA and 0–12 kPa H_2O, where the conversions of IPA dehydration were below 10%. In the absence of co-fed water, the propene formation rate at 260°C first increases and then plateaus with increasing IPA partial pressure on both TiO_2(101) and (001) (Figure 2A,B), where the intrinsic activity on TiO_2(101) is about two-fold higher than that on TiO_2(001), consistent with the prior report [31]. Introducing 2, 4, or 8 kPa

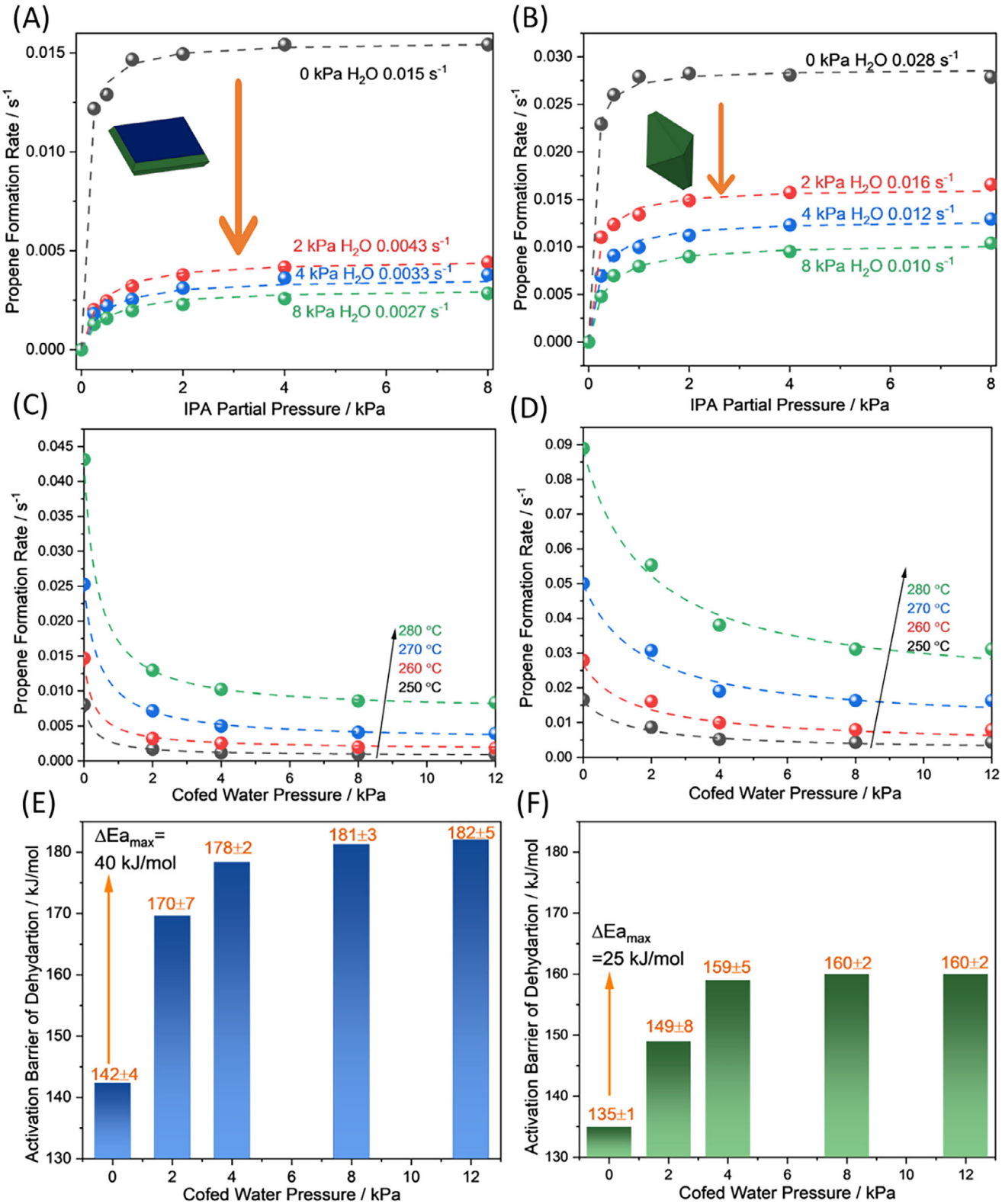

FIGURE 2 | Kinetic dependences of propene formation rates over (A) TiO_2(001) and (B) (101) on IPA and water pressures at 260°C; kinetic dependences of propene formation rates over (C) TiO_2(001) and (D) (101) on water at 250°C–280°C and 1 kPa IPA; activation barriers on (E) TiO_2(001) and (F) (101) at 0–12 kPa co-fed water and 1 kPa IPA. Operating conditions: 250°C–280°C, 1 atm total pressure with 0.25–8 kPa IPA, 0–8 kPa H_2O, and balance He, and 47.6 $cm^3\ g^{-1}\ s^{-1}$ gas hourly space velocity (GHSV). Dashed lines in (A)—(D) show the rates calculated based on parameters obtained from non-linear regression using Equation (1).

of H_2O into the feed of 8 kPa IPA, propene formation rates dramatically decreased by 3.5, 4.5, and 5.6 times, respectively, on TiO_2(001), and by 1.7, 2.3, and 2.8 times, respectively, on TiO_2(101). The larger rate drops on TiO_2(001) indicate the substantially stronger sensitivity of TiO_2(001) to water inhibition. Because the TiO_2(001) sample exposes ~60% (001) facets and ~40% (101) facets, while TiO_2(101) sample exposes ~93% of (101) facets and ~7% (001) facets, the measured rates reflect mixed-facet behavior. By extrapolating the rate to 100% (101) and 100% (001) surfaces, detailed in Figure S4 and SI Note 3, H_2O-induced rate suppression is about 3–5 times more severe on pure (001) than pure (101), indicating a more pronounced effect on the (001) surface. Since the partial pressure of co-fed water is orders of magnitude higher than in situ generated water as quantified in Tables S2 and S3, H_2O inhibition is primarily due to the excessive co-fed H_2O but not to the formed H_2O, which can be further corroborated by the 10%–20% decrease in dehydration rates when co-feeding only 0.2 kPa water (Figure S5). Figure 2C,D shows dehydration rates as a function of water partial pressure at 250–280°C and a constant IPA pressure of 1 kPa. Dehydration rates decrease with increasing water partial pressure on both facets and level off at roughly 8 kPa. This saturation behavior indicates water cannot displace surface-adsorbed IPA species but forms alcohol–water complexes that inhibit dehydration. At sufficiently high water and IPA partial pressures, these complexes become the most abundant surface intermediates that exhibit zero orders with respect to IPA and water (Figure 2A,B). From the extent of rate decrease, we again observe stronger water inhibition on TiO_2(001). Based on these kinetic data, we carried out Arrhenius analysis detailed in Figure S6; the resultant apparent activation barriers $E_{a,j}$ (subscript j = *001* or *101*, representing TiO_2(001) or TiO_2(101)) as a function of water pressure are depicted in Figure 2E,F. On TiO_2(001), $E_{a,001}$ increases from 142 ± 4 kJ mol^{-1} in the absence of co-fed H_2O, to 182 ± 5 kJ mol^{-1} at 12 kPa H_2O. While on TiO_2(101), $E_{a,101}$ increases from 135 ± 1 kJ mol^{-1} (0 kPa H_2O) to 160 ± 2 kJ mol^{-1} (12 kPa H_2O). The significantly larger increase in the apparent activation barriers on TiO_2(001) (40 kJ mol^{-1}) compared to TiO_2(101) (25 kJ mol^{-1}) quantitatively confirms the stronger water inhibition on the (001) facet. However, the rates decreased only 5.6 and 2.8-fold on TiO_2(001) and (101), respectively. Such modest reductions in rate, despite large enthalpic penalties, imply compensating increases in activation entropy. By using Arrhenius-based rate ratio expression and Eyring equation, the increases in activation entropy are 60 J mol^{-1} K^{-1} for TiO_2(001) and 35 J mol^{-1} K^{-1} for (101), detailed in Supporting Information: Note 4. The positive change in activation entropy indicates that the presence of water alters the nature of the transition state, increasing its configurational freedom relative to the dry condition, consistent with prior reports [44–46]. The larger entropy increase observed on TiO_2(001) compared to TiO_2(101) suggests that water perturbs the reactive surface intermediate more strongly on the (001) facet. However, the substantial elevation in activation enthalpy due to the dominant kinetic consequence of water leads overall to stronger net rate suppression.

Figure 3 presents temperature-programmed surface reaction (TPSR) results using various water introduction methods to probe the facet-dependent inhibition of IPA dehydration. On TiO_2(001) (Figure 3A), propene desorption temperature remains unchanged between IPA-only adsorption and sequential H_2O-IPA adsorption (blue trace), indicating that IPA displaces adsorbed H_2O. However, co-adsorption of IPA and H_2O leads to a ~6°C increase of propene desorption temperature, reflecting water inhibition. Furthermore, introducing H_2O (1 or 8 kPa) during temperature ramping leads to significant desorption temperature increasing from ~266 °C to 296 °C or 328 °C, signaling stronger inhibition. Such temperature shifts are indicative of an increased apparent activation barrier [47], consistent with steady-state kinetic data shown in Figure 2. TiO_2(101) (Figure 3B) shows similar trends: minimal changes in desorption temperature with different IPA/H_2O adsorption sequences (black and blue curves) but substantial increases when H_2O is present during temperature ramping. Notably, the inhibition effect is less pronounced compared to TiO_2(001), with propene desorption temperatures rising only from ~245 °C to 257 °C and 275 °C at 1 and 8 kPa H_2O, respectively. This difference corroborates the larger water-induced activation barrier increases on TiO_2(001) compared to TiO_2(101).

The steady-state and transient IPA dehydration kinetic results shown above clearly demonstrate more severe H_2O inhibition on TiO_2(001). Next, we performed high-vacuum IR to further exclude the contribution from competitive adsorption between IPA and H_2O. Four adsorption protocols were employed: (1) H_2O alone, (2) H_2O followed by IPA, (3) IPA alone, and (4) IPA followed by H_2O. On TiO_2(001) (Figure 3C), preheating at 400°C (red trace) results in a pronounced loss of the hydroxyls compared to the untreated one (black trace), indicating surface dehydroxylation. Exposure of the dehydrated surface to H_2O (blue trace) restores the bridging hydroxyls. Subsequent IPA dosing to the hydrated surface (yellow trace) produces intense ν(CH) bands (3000–2800 cm^{-1}) and a reduction in hydroxyls intensity. This is because at the initial transient state, IPA can react with surface hydroxyl groups, forming surface isopropoxide species and releasing water into the gas phase (Ti(OH) + C_3H_7OH = Ti(*i*-OC_3H_7) +H_2O) [31]. It is worth noting that the coverage of hydroxyl groups becomes dynamically constant after reaching the steady state during the reaction. When IPA is dosed first onto the preheated surface (green trace), similar ν(CH) intensities and hydroxyl consumption are observed. Subsequent H_2O dosing (purple trace) does not diminish the ν(CH) intensities, demonstrating that adsorbed IPA is not displaced by water. On TiO_2(101), the dehydrated surface (red trace) likewise exhibits diminished hydroxyl intensity compared to the untreated one (black trace). H_2O dosing (blue trace) restores bridging hydroxyls. Subsequent IPA dosing (yellow trace) produces strong ν(CH) bands and reduces hydroxyl intensity, with spectral features comparable to when IPA is dosed first (green trace). After adsorbing IPA, subsequent H_2O exposure (purple trace) does not attenuate the ν(CH) bands, indicating that IPA remains adsorbed. Even a tenfold higher H_2O pressure does not reduce IPA coverage (Figure S7). Notably, a red-shifted hydroxyl band at ~3480 cm^{-1} emerges upon IPA adsorption, indicating molecular IPA hydrogen-bonding with hydroxyls [31]. Upon co-adsorption of H_2O either before or after IPA, this hydroxyl feature blue-shifts from ~3473 to 3486 cm^{-1}, demonstrating that water perturbs the IPA–surface hydrogen bonding environment and interacts with co-adsorbed IPA, forming complexes. These results demonstrate that IPA exhibits stronger adsorption than H_2O on both TiO_2 facets. The observed ν(CH) intensities are unaffected by dosing sequence, confirming that competitive adsorption is excluded for contributing to the dehydration inhibition.

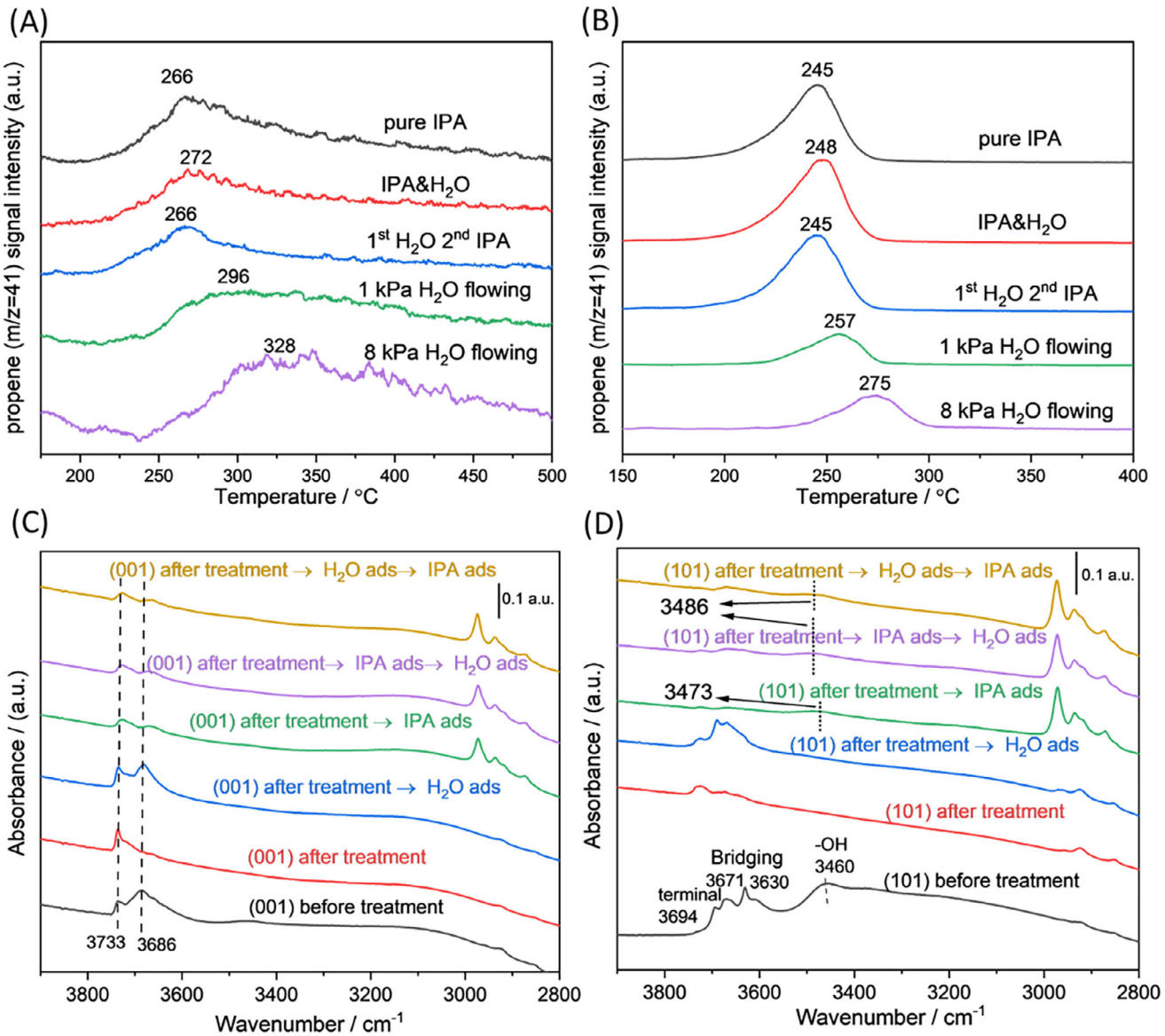

FIGURE 3 | IPA-TPSR with different ways of introducing water on (A) TiO_2(001) and (B) TiO_2(101). High vacuum IR by introducing IPA and H_2O with different sequences on (C) TiO_2(001) and (D) TiO_2(101). Operating conditions: (A), (B) TPSR of pretreated catalysts (450°C, 10% O_2/He, 1 h) was conducted in flowing He (25 mL min^{-1}) with 0 (black, red, blue), 1 (green) or 8 kPa (purple) H_2O after adsorption of IPA, H_2O, or H_2O:IPA mixture (3:2 partial pressure ratio) at 120°C; (C), (D) Pretreated catalysts (red; 450°C, 10^{-6} mbar, 1 h) were initially exposed to IPA (green; 0.1 mbar, 0.5 h), H_2O (blue; 0.1 mbar, 0.5 h), H_2O-to-IPA or IPA-to-H_2O [yellow or purple; exposure to 0.1 mbar H_2O (or IPA) for 0.5 h, then degassing at 10^{-6} mbar for 1 h, followed by exposure to 0.1 mbar IPA (or H_2O) for 0.5 h] at 100°C, followed by vacuum degassing at 10^{-6} mbar for 1 h before transmission IR measurements. Untreated catalysts (black) were degassed at 10^{-6} mbar for 1 h at 25°C.

2.3 | Probing IPA-H_2O Interactions via In Situ DRIFTS and NMR Spectroscopies

Having ruled out competitive adsorption, we employed in situ DRIFTS to investigate the effect of water on adsorption mode of IPA. As shown in Figure 4A, clean TiO_2(101) (bottom spectrum) presents terminal (3719 cm^{-1}) and bridging (3666 and 3636 cm^{-1}) hydroxyls [48, 49]. Weak features at ~3500 and 1615 cm^{-1} correspond to residue-adsorbed H_2O. A broad IR feature at about 3100 cm^{-1} is also observed for TiO_2(101). This significantly red-shifted OH band is characteristic of water molecules adsorbed via strong hydrogen bonding on oxide surfaces [50]. Upon IPA exposure at 100 °C, the original ν(OH) bands at 3636–3719 cm^{-1} largely disappear, and a new ν(OH) band emerges at 3450 cm^{-1}, attributed to molecular IPA adsorbed via hydrogen bonding to surface hydroxyls (i.e., Ti-OH⋯OH-C_3H_7-i), evidence by vacuum IR as well. Molecularly adsorbed IPA on Lewis acid sites (Ti_{5c} sites) is further supported by the in-plane δ(OH) band at 1285 cm^{-1} [51–54]. IPA adsorption also produces $\nu(CH_3)_{as}$ and $\nu(CH_3)_s$ bands within 3000–2800 cm^{-1}, as well as $\delta(CH_3)_{as}$ and $\delta(CH_3)_s$ bands at 1465 and 1385 cm^{-1}, respectively [51–53]. These vibrational features alone do not distinguish chemisorbed IPA from isopropoxide [53, 55]. It is noted that owing to the sloping baseline and overlap with other vibrational modes, the

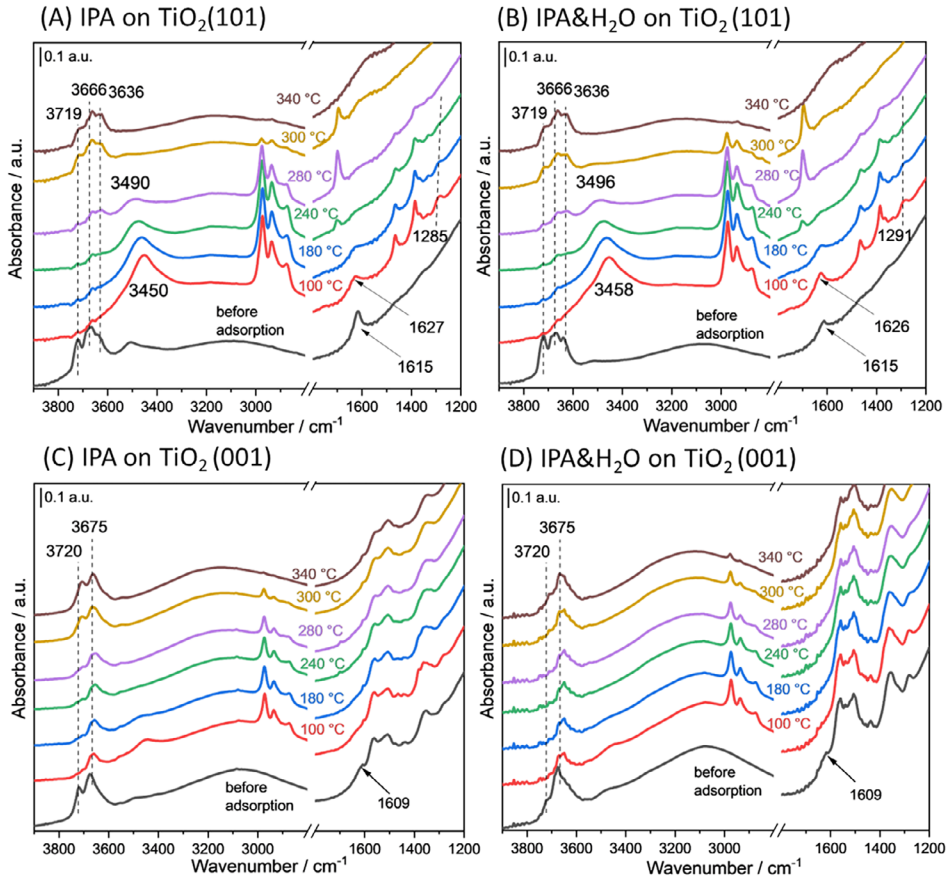

FIGURE 4 | (A) and (C) In situ DRIFTS-TPD spectra of adsorption and desorption of pure IPA on TiO_2(101) and (001); (B) and (D) in situ DRIFTS-TPD spectra of adsorption and desorption of 3:2 H_2O:IPA (partial pressure) on (101) and (001). Operating conditions: catalysts (20 mg) were pretreated in 10% O_2/He at 450°C under ambient pressure for 1 h, and then treated with IPA (A, C), or IPA and H_2O mixture (2:3 partial pressure ratio) (B, D) in flowing He at 100°C until saturation, followed by ramping from 100°C to 450°C (10°C min^{-1}) in flowing He (50 mL min^{-1}).

absorbance in the 1000–1200 cm^{-1} region provides only limited information about the C–O stretching vibrations. Notably, the H_2O bending mode weakens and blueshifts to 1627 cm^{-1} upon IPA adsorption, indicating partial displacement of pre-adsorbed water and interaction between the two adsorbates [48]. As temperature increases from 100 to 300 °C, all the IPA bands progressively diminish, suggesting molecular IPA dehydration on Lewis acid-base pairs via an E2 mechanism [31]. Figure 4B presents spectra acquired upon the co-adsorption of IPA and water. The perturbed ν(OH) band and in-plane δ(OH) band shift from 3450 to 3458 cm^{-1} and from 1285 to 1291 cm^{-1} respectively, indicating that water interacts with adsorbed IPA without altering its molecular adsorption mode. The key difference is that ν(CH) peaks vanish at 340°C higher than 320°C in the dry surface case, as shown by the slower decrease in ν(CH) peak areas in Figure S8A, indicating water inhibits dehydration activity, consistent with kinetic results. For pure water adsorption on the (101) facet (Figure S10), the perturbed ν(OH) band appears at 3467 cm^{-1}, blue shifting about 10 cm^{-1} compared to co-adsorption case. The shift demonstrates that surface water interacts with adsorbed IPA.

Figure 4C presents spectra with pure IPA adsorption on TiO_2(001) at 100°C, followed by heating. The clean TiO_2(001) displays terminal and bridging hydroxyls at 3720 and 3675 cm^{-1}. In contrast to TiO_2(101), a broad ν(OH) feature centered at ~3100 cm^{-1} is present together with weak H_2O bending mode at ~1609 cm^{-1}, indicating more rigid and ice-like H_2O on TiO_2(001) [56]. Upon IPA exposure, hydroxyls are partially consumed, accompanied by the appearance of ν(CH) bands. Unlike TiO_2(101), however, the characteristics of molecular IPA, perturbed ν(OH) (~3450 cm^{-1}) and δ(OH) (~1290 cm^{-1}) features, are barely detected. This indicates that IPA primarily adsorbs dissociatively as isopropoxide [31]. Upon heating, isopropoxide species are fully dehydrated by ~340°C, accompanied by regeneration of surface hydroxyls. Figure 4D presents spectra with co-adsorption of IPA and H_2O. Even at 340°C, characteristic isopropoxide bands remain detectable, indicating water retards isopropoxide dehydration. This inhibitory effect is further quantified by plotting ν(CH) peak area versus temperature (Figure S8B). Importantly, no molecular IPA features emerge under co-adsorption conditions, indicating that water suppresses isopropoxide dehydration without altering its dissociative adsorption mode. The 1699 cm^{-1} acetone feature is consistent with the trace acetone formed under steady-state reaction conditions; however, this minor byproduct does not affect our mechanistic conclusions regarding the dominant adsorbed species on the two facets.

While in situ DRIFTS provides valuable insight into facet-dependent adsorption modes, that is, molecular versus dissociative adsorption, its sensitivity is limited when probing more subtle interactions between IPA and co-adsorbed water. We further employed in situ ^{1}H–^{13}C CP and DP MAS NMR spectroscopies,

which offer higher sensitivity to the local environment, to probe the molecular-level interactions among IPA, water, and TiO_2 surfaces. Figure 5A,B presents ^1H-^{13}C CP spectra of IPA and water adsorbed on TiO_2(001) and (101). CP selectively detects strongly adsorbed species while suppressing signals from weakly bound or gas-phase molecules, a feature evident in Figure 5A, where spectra obtained after dosing TiO_2(001) with one or two monolayers (ML) of IPA appear nearly identical. A monolayer was defined as the number of surface-exposed Ti sites quantified by NH_3-TPD. Upon IPA adsorption, three CP resonances emerge at ~78, ~69, and ~24 ppm, corresponding to methine carbons of isopropoxide and molecular IPA and methyl groups of both, respectively [57], indicating that NMR allows direct differentiation between molecular IPA and isopropoxide. Deconvolution reveals that ~80% of adsorbed IPA adopts dissociative binding as isopropoxide, while ~20% remains molecular. With the addition of an equal amount of water, the intensity of the 78 ppm resonance markedly decreases and that of the 68 ppm peak increases while the total area of the two resonances is largely maintained. Since high-vacuum IR demonstrates no competitive adsorption, the 68 ppm resonance observed in the presence of 2 ML H_2O is unlikely to arise from molecular IPA but is more plausibly an isopropoxide–H_2O complex, as depicted in Figure 5E. Additionally, ~24 ppm methyl resonance became much sharper, indicating the faster molecular motion of the methyl group. Methine ^{13}C of IPA upshifting and a sharper methyl ^{13}C peak both indicate weaker surface binding of isopropoxide and a more disordered adsorbate environment with the presence of water, leading to a possibly loosened and disordered configuration.

In contrast, upon dosing TiO_2(101) with IPA (Figure 5B), adsorption is dominated by the molecular state at ~68 ppm (~70%), with a minor dissociative isopropoxide contribution of ~78 ppm (~30%), consistent with DRIFTS. Upon co-adsorption with H_2O, the dominant molecular IPA resonance shifts from ~68 to ~64 ppm. Since H_2O does not compete with IPA on TiO_2(101) either, this peak is assigned to a hydrogen-bonded molecular IPA complex. This assignment is corroborated by ^{13}C DP spectra at 12 ML IPA loadings (Figure S12C), which show a significantly sharp signal at ~64 ppm from weakly bound molecular IPA that is absent in ^1H–^{13}C CP, confirming the ~64 ppm CP resonance corresponds to hydrogen-bonded molecular IPA. A ~10 ppm shift on TiO_2(001) compared to a ~4 ppm shift on TiO_2(101) indicates a stronger interaction between isopropoxide-water on the (001) surface than IPA-water on the (101) surface. Again, the methine ^{13}C of IPA upshifting and a sharper methyl ^{13}C peak both indicate that water weakens the adsorption of molecular IPA on the surface and creates a more disordered adsorbate environment. We further conduct DFT-NMR to cross-validate the assignment of IPA species adsorbed. As shown in Figure S13, the isopropoxide resonates at 86.4 ppm, which upshifts by 5.3 to 81.1 ppm with the presence of one water molecule, shown in Models (B) and (C). In contrast, molecularly adsorbed IPA shifts from 71.8 by 1.8 to 70.0 ppm with the presence of water. These trends align with experimental observations, confirming that water perturbs isopropoxide more strongly than molecular IPA on two respective facets.

To further support this interpretation, we conduct ^1H MAS NMR (Figure 5C,D). Clean TiO_2(001) and (101) display terminal hydroxyls at ~1 ppm and bridging hydroxyls at ~6.5 ppm. TiO_2(001) exhibits an additional resonance at ~11 ppm, which has been assigned to bicarbonate species [58]. These species may originate from interactions between hydroxyl groups and CO_2 generated from urea decomposition during hydrothermal synthesis and subsequent calcination [59, 58]. However, because this resonance remains largely unchanged upon IPA and H_2O adsorption, it appears that these species interact minimally, if at all, with IPA or water under the conditions studied. Therefore, this feature is unlikely to significantly affect our main conclusions regarding the facet-dependent influence of distinct IPA–H_2O complexes on reaction kinetics. Upon IPA adsorption, the ~1 ppm signal increases and broadens relating to methyl groups of IPA, while the ~6.5 ppm resonance weakens and becomes less defined due to interacting with IPA through hydrogen bonding or forming isopropoxide, as illustrated in ^{13}C NMR and DRIFTS. Following the adsorption of 2 ML of H_2O, water proton resonances appear at 7.1 ppm on TiO_2(001) and 6.1 ppm on TiO_2(101). In contrast, H_2O adsorbed alone on the clean surfaces yields resonances at 5.8 and 5.4 ppm, respectively. The larger downfield shift observed on TiO_2(001) (Δ = 1.3 ppm) compared to TiO_2(101) (Δ = 0.7 ppm) indicates a stronger deshielding effect by neighboring IPA/isopropoxide, indicating stronger hydrogen bonding between H_2O and the oxygen of isopropoxide on the (001) facet. In comparison, the smaller shift on TiO_2(101) suggests weaker hydrogen bonding between H_2O and molecular IPA. Combining ^1H-^{13}C CP and ^{13}C and ^1H DP NMR, we propose that water interacts with isopropoxide on TiO_2(001) to form an isopropoxide-H_2O complex intermediate (Figure 5E). In contrast, H_2O interacts weakly with molecular IPA on (101) to form hydrogen-bonded molecular IPA intermediate (Figure 5F). Next, we apply DFT calculations and kinetic analysis to support such structure models and discuss how this molecular-level knowledge helps to better understand H_2O inhibition in acid-base catalysis.

2.4 | Mechanistic Considerations of Facet-Dependent Inhibition From DFT Calculations and Kinetic Studies

Previous studies have established that IPA dehydration on TiO_2 prefers to undergo via an E2 elimination mechanism, where the rate-limiting step is concurrent C-H and C-O bond cleavages [31, 60]. To reveal potential changes of reaction mechanism under H_2O inhibition, we carried out kinetic isotope effect (KIE) measurements using $CD_3CH(OH)CD_3$ or $CH_3CH(OD)CH_3$ at 260°C. As demonstrated in Table S4, when hydroxyl hydrogen is deuterated, KIEs are approximately unity on both TiO_2(001) and (101), regardless of the presence or absence of co-fed water, indicating no isotope effect. However, when C_β-H are deuterated, KIEs are close to 2 on both TiO_2(101) and (001) with and without co-fed water. These results suggest that the reaction in the presence of water still follows the E2 mechanism.

Besides, since in situ DRIFTS and NMR spectroscopies consistently demonstrate that IPA adsorbs predominantly molecularly on TiO_2(101) and dissociatively on TiO_2(001) with water addition not altering these adsorption modes, DFT calculations were performed to corroborate these assignments and to rationalize the facet-dependent water inhibition mechanisms observed experimentally. According to the previous study [31], Ti-O_s-Ti(OH) and Ti-O_s are proposed as active sites on TiO_2(001) and (101),

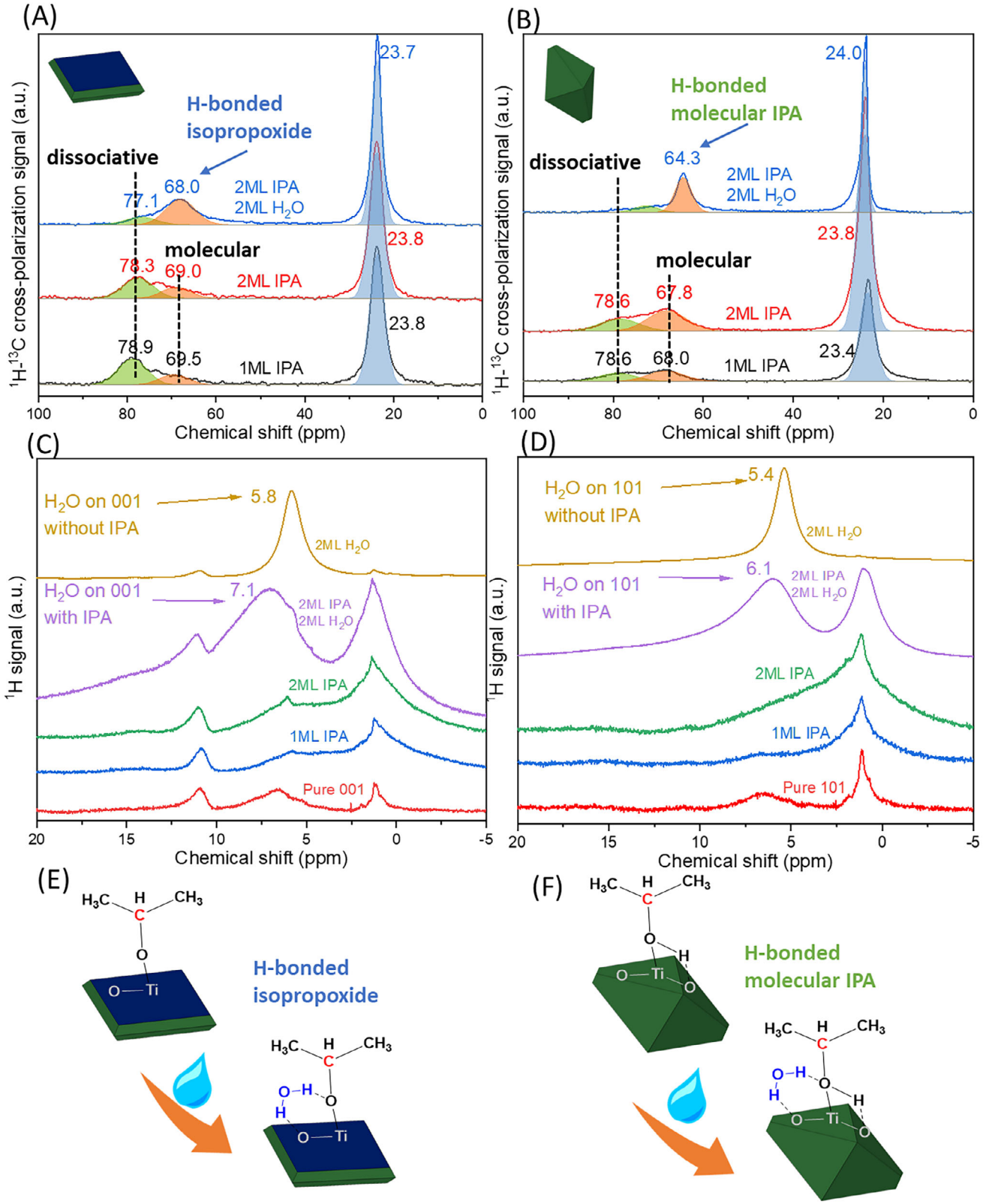

FIGURE 5 | (A) and (B) in situ ^{1}H-^{13}C CP NMR of IPA and water adsorbed on (001) and (101); (C) and (D) in situ ^{1}H DP NMR of IPA and water adsorbed on TiO_2(001) and (101); (E) and (F) representative scheme of isopropoxide-H_2O complex on (001) and IPA-H_2O complex on (101). Operating conditions: catalysts (100 mg) were pretreated in 10% O_2/He at 450°C under ambient pressure for 1 h. The required amount of IPA and H_2O liquids were injected onto the samples inside NMR rotor in the glovebox via μL syringes.

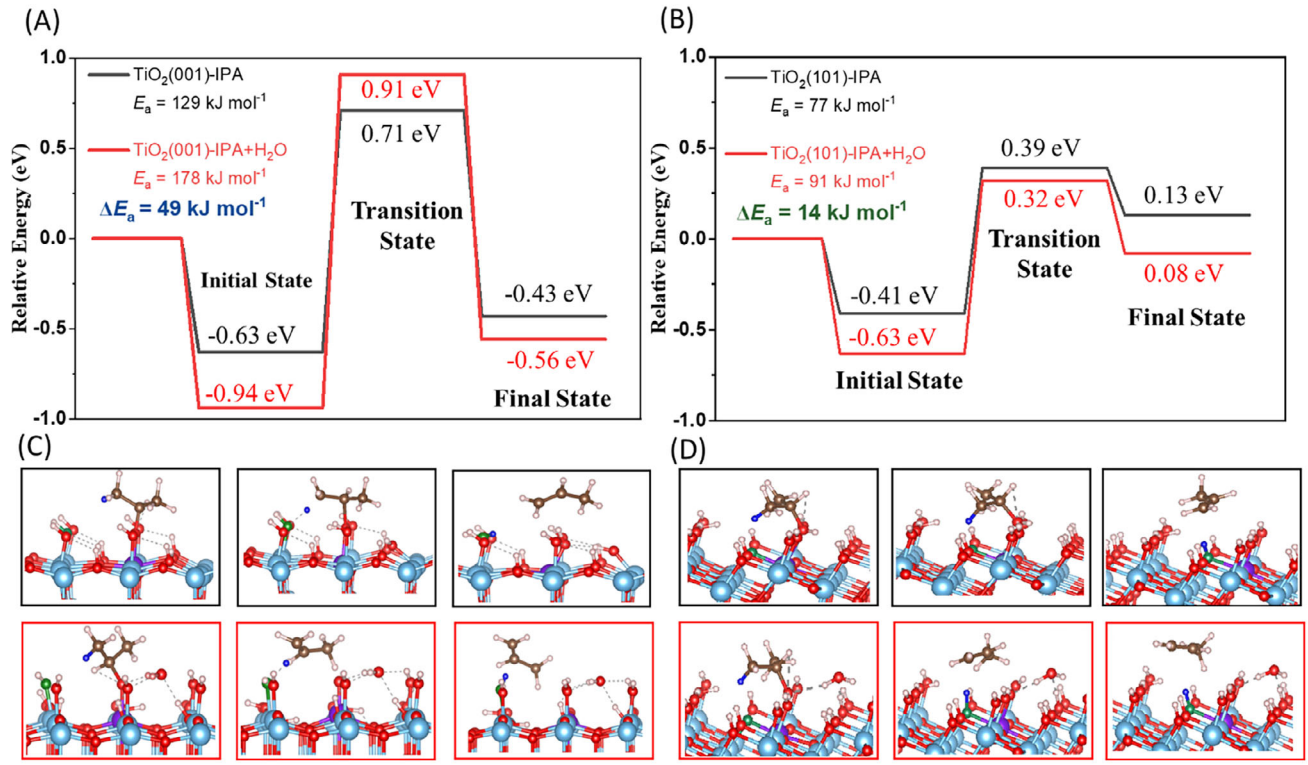

FIGURE 6 | DFT calculations of reaction pathway and activation energy of IPA dehydration with and without water on (A) TiO_2(001) and (B) TiO_2(101). Initial, transition, and final states models with and without water on (C) TiO_2(001) and (D) TiO_2(101).

respectively. As shown in Figure 6A,C, IPA dissociates spontaneously on active sites (Ti-O_s-Ti(OH)) of (001) surface, forming Ti(*i*-OC_3H_7)-O_s(H)-Ti(OH), where the Ti-O bond distance in the Ti(*i*-OC_3H_7) moiety is 1.8 Å, and the C_β-C_α-Ti angle is 109°, that is, the carbon chain lies relatively parallel to the surface, as depicted in Figure S14A. The transition state is formed by Ti-OH···H-C_β interactions with a computed activation barrier of 129 kJ mol^{-1}. The simultaneous C-H and C-O cleavage of this transition state (i.e., E2 dehydration) yields propene and water. In the presence of an H_2O molecule, it interacts with Ti(*i*-OC_3H_7) via hydrogen bonding through the O atom of isopropoxide, according to NMR analysis. The H-O-H···O-Ti hydrogen bond distance is 1.84 Å, that is, a relatively strong hydrogen bonding, consistent with ^{1}H NMR. It is also worth noting that (1) the Ti-O bond distance of the intermediate is elongated from 1.80 to 1.88 Å upon water coordination and (2) the C_β-C_α-Ti angle is enlarged to 122° (Figure S14B), consistent with NMR results that the H_2O molecule pushes methyl groups away from the (001) surface. Consequently, the methyl groups tilt away from the TiO_2(001) surface. This geometric distortion reflects the weakened adsorption of the reacting isopropoxide species, which makes the transition state less stabilized by the surface, leading to a markedly higher activation energy of 179 kJ mol^{-1}. The activation barrier difference of 50 kJ mol^{-1} resulting from water inhibition is consistent with experimental results (40 kJ mol^{-1}) shown in Figure 2E. Although entropy was not explicitly evaluated in the DFT calculations, the predicted geometric relaxation and reduced surface confinement are consistent with the experimentally observed increase in activation entropy. Formation of the isopropoxide–water complex weakens the rigidity of the adsorbed species and likely induces greater configurational flexibility in the transition state. Thus, the DFT results support a mechanistic picture where water destabilizes the transition state with an increasing structural disorder.

Figure 6B,D presents the energy profile of the E2 elimination step and the corresponding models on the (101) surface, respectively. For the molecular adsorbed Ti(IPA)-O_s, the Ti-O distance in the Ti(IPA) moiety is 2.12 Å, obviously longer than isopropoxide on TiO_2(001). The two C_β-C_α-Ti bond angles are 94° and 95°, parallel to the (101) surface (Figure S14C). The transition state is stabilized by lattice O_s and Ti, derived from previous reported models [31]. The calculated activation energy is 77 kJ/mol, lower than that on the (001) surface, in agreement with kinetic measurements and prior theoretical studies [31]. After introducing an H_2O molecule, the Ti-O distance of the Ti(IPA···H_2O) moiety is elongated to 2.21 Å and two C_β-C_α-Ti angles expand to 97 and 137°, indicating partial tilting of one methyl group away from the surface (Figure S14D). The hydrogen bond distance of H-O-H···O-Ti in the Ti(IPA···H_2O) moiety is 2.15 Å, much longer than the hydrogen bond distance (1.84 Å) found on (001) surface. As such, the much weaker water inhibition on TiO_2(101) only leads to an increase in activation energy of E2 elimination of 14 kJ mol^{-1}, which is also in line with experimental data (25 kJ mol^{-1}). The geometry of the (101) surface and its preference for molecular IPA adsorption likely limit the perturbance degree of water on the reactive intermediate, thereby reducing its influence on the transition state. Although entropy was not explicitly calculated, the relatively small structural distortion upon water coordination suggests a smaller increase in configurational flexibility of the transition state, consistent with the smaller experimental increase in activation entropy compared to the (001) case.

The combination of kinetic studies, in situ DRIFTS and NMR characterizations, isotope studies, as well as DFT calculations, allows us to elucidate the elementary steps of IPA dehydration on TiO_2(001) and (101), as depicted in Tables S5 and S6. On TiO_2(001), the reaction initiates with the dissociative adsorption of IPA, forming isopropoxide (Ti(i-OC_3H_7)-O_s(H)-Ti(OH), **Step (001)-1**). Meanwhile, the molecular adsorption of H_2O generates Ti(H_2O)-O_s-Ti(OH) species (**Step (001)-2**). The adsorbed species can interact with another gaseous H_2O molecule, forming an isopropoxide-water complex (Ti(i-OC_3H_7···H_2O)-O_s(H)-Ti(OH), **Step (001)-3**) or a water dimer (Ti(H_2O)$_2$-O_s-Ti(OH), **Step (001)-4**). Subsequently, the kinetically relevant E2 elimination occurs via the attack of the OH to the C_β-H of the i-OC_3H_7 moiety and the simultaneous C-O bond cleavage, releasing propene into the gas phase (**Steps (001)-m-5** and **(001)-d-5**, where m and d denote monomeric and complex pathways, respectively). Finally, active sites are regenerated by the desorption of H_2O (**Steps (001)-m-6** and **(001)-d-6**).

On TiO_2(101), the reaction begins with molecular adsorptions of IPA or H_2O on Ti-O_s, forming Ti(IPA)-O_s (**Step (101)-1**) and Ti(H_2O)-O_s species (**Step (101)-2**), respectively, which can interact with another H_2O molecule to generate a IPA-water complex (Ti(IPA···H_2O)-O_s), **Step (101)-3**) or a water dimer (Ti(H_2O)$_2$-O_s), **Step (101)-4**). Subsequently, Ti(IPA)-O_s and Ti(IPA···H_2O)-O_s undergo via E2 elimination by the attack of O_s to the C_β-H of the IPA moiety and by the simultaneous C-O bond cleavage, producing gaseous propene (**Steps (101)-m-5** and **(101)-d-5**, respectively). Finally, the desorption of H_2O regenerates the Ti-O_s active sites to complete the catalytic cycle (**Steps (101)-m-6** and **(101)-d-6**).

Since the E2 elimination is the kinetically relevant step for both monomeric (**Steps (001)-m-5** and **(101)-m-5**) and complex pathways (**Steps (001)-d-5** and **(101)-d-5**), the pseudo steady-state approximation of all surface species leads to the following rate expression with the detailed derivation provided in Supporting Information: Note 5,

$$r_j = r_{m,j} + r_{d,j} = \frac{k_{m,j}K_{I,j}\,[IPA] + k_{d,j}K_{W\cdot D,j}K_{I,j}\,[IPA]\,[H_2O]}{1 + K_{I,j}\,[IPA] + K_{W1,j}\,[H_2O] + K_{W2,j}[H_2O]^2 + K_{W\cdot D,j}K_{I,j}\,[IPA]\,[H_2O]} \quad (1)$$

where $k_{m,j}$ and $k_{d,j}$ are the rate constants for monomer and complex; $K_{I,j}$, $K_{w1,j}$ $K_{w\cdot D,j}$ are the equilibrium constants for **Steps (j)-1**, **(j)-2**, and **(j)-3**, respectively; and $K_{w2,j}$ is the overall equilibrium constants for **Steps (j)-2 and (j)-4**. Nonlinear regression of the measured data to Equation (1) yields the parameters shown in Table S7, with the parity plots and sensitivity analysis provided in Figures S15–S17. Fitted results presented as dashed lines in Figure 2 match well with experimental data.

On TiO_2(001), the rate constant of the monomeric pathway ($k_{m,001}$) is 1.56 (± 0.17) × 10^{-2} s^{-1}, which is 6.3 times higher than that of the complex pathway ($k_{d,001}$), 2.49 (± 0.15) × 10^{-3} s^{-1}. Distinctively, on TiO_2(101), $k_{m,101}$ and $k_{d,101}$ are 2.87 (± 0.03) × 10^{-2} and 7.10 (± 0.90) × 10^{-3} s^{-1}, respectively, with the $k_{m,101}(k_{d,101})^{-1}$ ratio of 4.0. The larger $k_{m,001}(k_{d,001})^{-1}$ than $k_{m,101}(k_{d,101})^{-1}$ ratio agrees with the larger activation barrier difference on TiO_2(001) than on TiO_2(101). The $k_{m,101}(k_{m,001})$ ratio of 1.8 indicates that the monomeric pathway is easier to occur on TiO_2(101) than on TiO_2(001), agreeing with the lower activation barrier shown in Figure 2E,F, since molecularly adsorbed IPA on (101) is more favorable to dehydration than dissociatively adsorbed IPA on (001) [31]. Besides, the much larger $K_{w\cdot D,j}$ simulated on TiO_2(001) than on TiO_2(101) is consistent with the stronger adsorption energy of the isopropoxide-water complex on the former than that of the IPA-water complex on the latter. As shown in Table S8, for the coverage of the complex at 2–8 kPa H_2O, although it is similar on both facets at low IPA pressures (0.25-1 kPa), it is higher on TiO_2(001) (72%-91%) than on TiO_2(101) (54%–82%) at higher IPA pressures (2-8 kPa IPA). Besides, the complex pathway becomes dominant ($r_{d,j}(r_{m,j})^{-1} > 1$) at above 2.3 kPa and 5.8 kPa H_2O on TiO_2(001) and (101), respectively, indicating that TiO_2(001) is more sensitive to the co-fed water. Collectively, the stronger water inhibition on IPA dehydration rates on TiO_2(001) arises from both a greater suppression of the rate constant of the complex pathway and the dominant surface coverage of isopropoxide-water species in a wide range of operating conditions.

3 | Conclusion

Unraveling how water influences alkanol dehydration is critical for advancing biomass upgrading under realistic and water-rich conditions. By exploiting TiO_2 facet engineering to minimize surface heterogeneity, this work provides an unambiguous molecular-level picture of how water inhibits IPA dehydration in a facet-dependent manner. We demonstrate that water suppresses the IPA dehydration rate on TiO_2(001) surface much more severely than on TiO_2(101), revealing fundamentally distinct inhibition mechanisms. Spectroscopic and kinetic analyses rule out competitive adsorption as an inhibition contributor. Instead, combined in situ IR, in situ NMR, kinetic studies, and DFT calculations reveal that water interacts strongly with dissociatively adsorbed isopropoxide on TiO_2(001), forming an isopropoxide–H_2O complex that readily drives the surface into a complex-dominated regime and generates a more disordered and loosely bound transition state, which can greatly elevate the barrier by 40 kJ mol^{-1}. In contrast, on TiO_2(101), water interacts only weakly with molecularly adsorbed IPA through hydrogen bonding with much lower coverages, leading to a smaller complex formation constant and a much smaller increase in the activation barrier (25 kJ mol^{-1}). This work identifies facet-dependent solvation of surface intermediates as a control parameter, demonstrating that water can fundamentally reshape activation barriers in a facet-specific manner and offering a new conceptual basis for catalyst design under realistic and water-rich conditions.

Author Contributions

Wenda Hu: writing – original draft, investigation, methodology, writing – review and editing. **Haiting Cai:** writing – original draft, formal analysis, data curation, writing – review and editing. **Anthony Savoy:** investigation, methodology, software. **Jinshu Tian:** data curation, formal analysis, visualization. **Sungmin Kim:** investigation, resources. **Fan Lin:** methodology, investigation. **Junrui Li:** methodology, validation. **Hao Xu:** formal analysis. **Yiqing Wu:** methodology. **Zihao Zhang:** writing – review and editing. **Nicholas Jaegers:** methodology, writing – review and editing, resources, software. **Feng Gao:** supervision, writing – review and editing, resources. **Huamin Wang:** resources, conceptualization, supervision. **Jianzhi Hu:** supervision, writing – review and editing, resources, funding acquisition, conceptualization. **Yong Wang:** supervision, writing – review and editing, resources, funding acquisition, conceptualization, project administration.

Acknowledgments

This work was supported by the U.S. Department of Energy (DOE), Office of Science (SC), Basic Energy Sciences (BES), Division of Chemical Sciences, Geosciences, and Biosciences within the Catalysis Science program (DE-AC05-RL01830, FWP-47319). We thank Pacific Northwest National Laboratory (PNNL), a multiprogram national laboratory operated for the DOE by Battelle for all the characterizations. Part of the work was conducted in the William R. Wiley Environmental Molecular Sciences Laboratory (EMSL), a national scientific user facility sponsored by DOE's Office of Biological and Environmental Research located at PNNL.

Conflicts of Interest

The authors declare no conflicts of interest.

Data Availability Statement

The data that support the findings of this study are available from the corresponding author upon reasonable request.

References

1. P. Gallezot, "Conversion of Biomass to Selected Chemical Products," *Chemical Society Reviews* 41 (2012): 1538–1558, https://doi.org/10.1039/C1CS15147A.

2. A. Corma, S. Iborra, and A. Velty, "Chemical Routes for the Transformation of Biomass Into Chemicals," *Chemical Reviews* 107 (2007): 2411–2502, https://doi.org/10.1021/cr050989d.

3. T. W. Walker, A. K. Chew, H. Li, et al., "Universal Kinetic Solvent Effects in Acid-Catalyzed Reactions of Biomass-Derived Oxygenates," *Energy & Environmental Science* 11 (2018): 617–628, https://doi.org/10.1039/C7EE03432F.

4. J. C. Serrano-Ruiz and J. A. Dumesic, "Catalytic Routes for the Conversion of Biomass Into Liquid Hydrocarbon Transportation Fuels," *Energy & Environmental Science* 4 (2011): 83–99, https://doi.org/10.1039/C0EE00436G.

5. Y. Roman-Leshkov, C. J. Barrett, Z. Y. Liu, and J. A. Dumesic, "Production of Dimethylfuran for Liquid Fuels From Biomass-Derived Carbohydrates," *Nature* 447 (2007): 982–985, https://doi.org/10.1038/nature05923.

6. F. Cavani, S. Guidetti, L. Marinelli, M. Piccinini, E. Ghedini, and M. Signoretto, "The Control of Selectivity in Gas-Phase Glycerol Dehydration to Acrolein Catalysed by Sulfated Zirconia" *Applied Catalysis B: Environmental* 100 (2010): 197.

7. G. Centi, R. K. Grasselli, and F. Trifiro, "Propane ammoxidation to acrylonitrile - an overview," *Catalysis Today* 13 (1992): 661–666, https://doi.org/10.1016/0920-5861(92)80106-W.

8. V. S. Sikarwar, M. Zhao, P. Clough, et al., "An Overview of Advances in Biomass Gasification," *Energy & Environmental Science* 9 (2016): 2939–2977, https://doi.org/10.1039/C6EE00935B.

9. Z. Buniazet, J. Couble, D. Bianchi, et al., "Unravelling Water Effects on Solid Acid Catalysts: Case Study of TiO_2/SiO_2 as a Catalyst for the Dehydration of Isobutanol," *Journal of Catalysis* 348 (2017): 125–134, https://doi.org/10.1016/j.jcat.2016.12.007.

10. Q. Wei, C. Yu, X. Song, et al., "Recognition of Water-Induced Effects toward Enhanced Interaction Between Catalyst and Reactant in Alcohol Oxidation," *Journal of the American Chemical Society* 143 (2021): 6071–6078, https://doi.org/10.1021/jacs.0c10618.

11. K. Chen, J. Damron, C. Pearson, D. Resasco, L. Zhang, and J. L. White, "Zeolite Catalysis: Water Can Dramatically Increase or Suppress Alkane C–H Bond Activation," *ACS Catalysis* 4 (2014): 3039–3044, https://doi.org/10.1021/cs500858d.

12. K. Chen, A. Gumidyala, M. Abdolrhamani, C. Villines, S. Crossley, and J. L. White, "Trace Water Amounts Can Increase Benzene H/D Exchange Rates in an Acidic Zeolite," *Journal of Catalysis* 351 (2017): 130–135, https://doi.org/10.1016/j.jcat.2017.04.026.

13. M. Nielsen, A. Hafreager, R. Y. Brogaard, et al., "Collective Action of Water Molecules in Zeolite Dealumination," *Catalysis Science & Technology* 9 (2019): 3721–3725, https://doi.org/10.1039/C9CY00624A.

14. Y. Dai, G. Li, D. E. Resasco, and Y. Yang, "How Do Structure and Topology of the Catalyst Affect Water Promotion or Inhibition Effects?," *Chemistry Catalysis* 1 (2021): 962–965, https://doi.org/10.1016/j.checat.2021.09.006.

15. G. Li, Y. Dai, Y. Yang, and D. E. Resasco, "Can We Predict Whether Water Will Inhibit or Enhance a Given Catalytic Reaction?," *Chemistry Catalysis* 1 (2021): 959–961, https://doi.org/10.1016/j.checat.2021.09.005.

16. S. Roy, G. Mpourmpakis, D.-Y. Hong, D. G. Vlachos, A. Bhan, and R. J. Gorte, "Mechanistic Study of Alcohol Dehydration on γ-Al_2O_3," *ACS Catalysis* 2 (2012): 1846–1853, https://doi.org/10.1021/cs300176d.

17. Y. Zhi, H. Shi, L. Mu, et al., "Dehydration Pathways of 1-Propanol on HZSM-5 in the Presence and Absence of Water," *Journal of the American Chemical Society* 137 (2015): 15781–15794, https://doi.org/10.1021/jacs.5b09107.

18. F. Lin, W. Hu, N. R. Jaegers, et al., "Elucidation of the Roles of Water on the Reactivity of Surface Intermediates in Carboxylic Acid Ketonization on TiO_2," *Journal of the American Chemical Society* 145 (2023): 99–109, https://doi.org/10.1021/jacs.2c08511.

19. J. Macht, M. J. Janik, M. Neurock, and E. Iglesia, "Mechanistic Consequences of Composition in Acid Catalysis by Polyoxometalate Keggin Clusters," *Journal of the American Chemical Society* 130 (2008): 10369–10379, https://doi.org/10.1021/ja803114r.

20. J. F. DeWilde, H. Chiang, D. A. Hickman, C. R. Ho, and A. Bhan, "Kinetics and Mechanism of Ethanol Dehydration on γ-Al_2O_3: The Critical Role of Dimer Inhibition," *ACS Catalysis* 3 (2013): 798–807, https://doi.org/10.1021/cs400051k.

21. M. Kang and A. Bhan, "Kinetics and Mechanisms of Alcohol Dehydration Pathways on Alumina Materials," *Catalysis Science & Technology* 6 (2016): 6667–6678, https://doi.org/10.1039/C6CY00990E.

22. M. Vyas, L. Patterson, and S. Kwon, "Alkanol Dehydration and Dehydrogenation Pathways on Anatase TiO_2 Under Oxidative and Nonoxidative Conditions," *Journal of Catalysis* 452 (2025): 116414, https://doi.org/10.1016/j.jcat.2025.116414.

23. K. Nakajima, Y. Baba, R. Noma, et al., "$Nb_2O_5 \cdot nH_2O$ as a Heterogeneous Catalyst With Water-Tolerant Lewis Acid Sites," *Journal of the American Chemical Society* 133 (2011): 4224–4227, https://doi.org/10.1021/ja110482r.

24. M. Wang, N. R. Jaegers, M.-S. Lee, et al., "Genesis and Stability of Hydronium Ions in Zeolite Channels," *Journal of the American Chemical Society* 141 (2019): 3444–3455, https://doi.org/10.1021/jacs.8b07969.

25. J. S. Bates, B. C. Bukowski, J. Greeley, and R. Gounder, "Structure and Solvation of Confined Water and Water–Ethanol Clusters Within Microporous Brønsted Acids and Their Effects on Ethanol Dehydration Catalysis," *Chemical Science* 11 (2020): 7102–7122, https://doi.org/10.1039/D0SC02589E.

26. G. Liu, J. C. Yu, G. Q. Lu, and H.-M. Cheng, "Crystal Facet Engineering of Semiconductor Photocatalysts: Motivations, Advances and Unique Properties," *Chemical Communications* 47 (2011): 6763, https://doi.org/10.1039/c1cc10665a.

27. J. E. Rekoske and M. A. Barteau, "Kinetics and Selectivity of 2-Propanol Conversion on Oxidized Anatase TiO_2," *Journal of Catalysis* 165 (1997): 57, https://doi.org/10.1006/jcat.1997.1467.

28. G. Pérez-López, R. Ramírez-López, and T. Viveros, "Acidic properties of Si- and Al- promoted TiO_2 catalysts: Effect on 2-propanol dehydration activity," *Catalysis Today* 305 (2018): 182.

29. D. Haffad, A. Chambellan, and J. C. Lavalley, "Propan-2-ol Transformation on Simple Metal Oxides TiO_2, ZrO_2 and CeO_2," *Journal of Molecular Catalysis A: Chemical* 168 (2001): 153–164, https://doi.org/10.1016/S1381-1169(00)00516-1.

30. M. Badlani and I. E. Wachs, "Methanol: A 'Smart' Chemical Probe Molecule," *Catalysis Letters* 75 (2001): 137–149, https://doi.org/10.1023/A:1016715520904.

31. F. Lin, Y. Chen, L. Zhang, et al., "Single-Facet Dominant Anatase TiO_2 (101) and (001) Model Catalysts to Elucidate the Active Sites for Alkanol Dehydration," *ACS Catalysis* 10 (2020): 4268–4279, https://doi.org/10.1021/acscatal.9b04654.

32. G. S. Foo, G. Hu, Z. D. Hood, M. Li, D.-E. Jiang, and Z. Wu, "Kinetics and Mechanism of Methanol Conversion Over Anatase Titania Nanoshapes," *ACS Catalysis* 7 (2017): 5345–5356, https://doi.org/10.1021/acscatal.7b01456.

33. F. Lin, H. Wang, Y. Zhao, et al., "Elucidation of Active Sites in Aldol Condensation of Acetone Over Single-facet Dominant Anatase TiO_2 (101) and (001) Catalysts," *JACS Au* 1 (2020): 41–52, https://doi.org/10.1021/jacsau.0c00028.

34. F. Xiong, Y. Y. Yu, Z. Wu, et al., "Methanol Conversion Into Dimethyl Ether on the Anatase TiO_2 (001) Surface," *Angewandte Chemie* 55 (2016): 623–628, https://doi.org/10.1002/anie.201509021.

35. A. Ignatchenko, D. G. Nealon, R. Dushane, and K. Humphries, "Interaction of Water With Titania and Zirconia Surfaces," *Journal of Molecular Catalysis A: Chemical* 256 (2006): 57–74, https://doi.org/10.1016/j.molcata.2006.04.031.

36. W. Yuan, B. Zhu, X.-Y. Li, et al., "Visualizing H_2O Molecules Reacting at TiO_2 Active Sites with Transmission Electron Microscopy," *Science* 367 (2020): 428–430, https://doi.org/10.1126/science.aay2474.

37. Y. K. Kim, R. Rousseau, B. D. Kay, J. M. White, and Z. Dohnálek, "Catalytic Dehydration of 2-Propanol on $(WO_3)_3$ Clusters on TiO_2(110)," *Journal of the American Chemical Society* 130 (2008): 5059–5061, https://doi.org/10.1021/ja800730g.

38. P. Zhang, J. Xiong, Y. Wei, et al., "Exposed {0 0 1} Facet of Anatase TiO_2 Nanocrystals in Ag/TiO_2 Catalysts for Boosting Catalytic Soot Combustion: The Facet-Dependent Activity," *Journal of Catalysis* 398 (2021): 109–122, https://doi.org/10.1016/j.jcat.2021.04.015.

39. C. E. Nanayakkara, W. A. Larish, and V. H. Grassian, "Titanium Dioxide Nanoparticle Surface Reactivity With Atmospheric Gases, CO_2, SO_2, and NO_2: Roles of Surface Hydroxyl Groups and Adsorbed Water in the Formation and Stability of Adsorbed Products," *Journal of Physical Chemistry C* 118 (2014): 23011–23021, https://doi.org/10.1021/jp504402z.

40. X. Han, X. Wang, S. Xie, et al., "Carbonate Ions-Assisted Syntheses of Anatase TiO_2 Nanoparticles Exposed With High Energy (001) Facets," *RSC Advances* 2 (2012): 3251–3253, https://doi.org/10.1039/C2RA00834C.

41. Y. K. Peng, Y. Hu, H. L. Chou, et al., "Mapping Surface-Modified Titania Nanoparticles With Implications for Activity and Facet Control," *Nature Communications* 8 (2017): 675, https://doi.org/10.1038/s41467-017-00619-z.

42. Y. Wu, F. Gao, H. Wang, L. Kovarik, B. Sudduth, and Y. Wang, "Probing Acid–Base Properties of Anatase TiO_2 Nanoparticles With Dominant {001} and {101} Facets Using Methanol Chemisorption and Surface Reactions," *Journal of Physical Chemistry C* 125 (2021): 3988–4000, https://doi.org/10.1021/acs.jpcc.0c11107.

43. L. Ye, J. Mao, J. Liu, Z. Jiang, T. Peng, and L. Zan, "Synthesis of Anatase TiO_2 Nanocrystals With {101},{001} or {010} Single Facets of 90% Level Exposure and Liquid-Phase Photocatalytic Reduction and Oxidation Activity Orders," *Journal of Materials Chemistry A* 1 (2013): 10532–10537, https://doi.org/10.1039/C3TA11791J.

44. Q. Liu and J. A. van Bokhoven, "Water Structures on Acidic Zeolites and Their Roles in Catalysis," *Chemical Society Reviews* 53 (2024): 3065–3095, https://doi.org/10.1039/D3CS00404J.

45. Y. Liu, A. Vjunov, H. Shi, et al., "Enhancing the Catalytic Activity of Hydronium Ions Through Constrained Environments," *Nature Communications* 8 (2017): 14113, https://doi.org/10.1038/ncomms14113.

46. L. Milakovic, P. H. Hintermeier, Y. Liu, E. Barath, and J. A. Lercher, "Influence of Intracrystalline Ionic Strength in MFI Zeolites on Aqueous Phase Dehydration of Methylcyclohexanols," *Angewandte Chemie* 60 (2021): 24806–24810, https://doi.org/10.1002/anie.202107947.

47. B. Sudduth, D. Yun, J. Sun, and Y. Wang, "Facet-Dependent Selectivity of CeO_2 Nanoparticles in 2-Propanol Conversion," *Journal of Catalysis* 404 (2021): 96–108, https://doi.org/10.1016/j.jcat.2021.09.009.

48. G. Jeantelot, S. Ould-Chikh, J. Sofack-Kreutzer, et al., "Morphology Control of Anatase TiO_2 for Well-Defined Surface Chemistry," *Physical Chemistry Chemical Physics* 20 (2018): 14362–14373, https://doi.org/10.1039/C8CP01983E.

49. H. Lin, J. Long, Q. Gu, et al., "In Situ IR Study of Surface Hydroxyl Species of Dehydrated TiO_2: Towards Understanding Pivotal Surface Processes of TiO_2 Photocatalytic Oxidation of Toluene," *Physical Chemistry Chemical Physics* 14 (2012): 9468, https://doi.org/10.1039/c2cp40893g.

50. S. Hosseinpour, F. Tang, F. Wang, et al., "Chemisorbed and Physisorbed Water at the TiO_2/Water Interface," *Journal of Physical Chemistry Letters* 8 (2017): 2195–2199, https://doi.org/10.1021/acs.jpclett.7b00564.

51. F. Kooli, C. Martín, and V. Rives, "FT-IR Spectroscopy Study of Surface Acidity and 2-Propanol Decomposition on Mixed Oxides Obtained Upon Calcination of Layered Double Hydroxides," *Langmuir* 13 (1997): 2303–2306, https://doi.org/10.1021/la960583j.

52. M. I. Zaki, M. A. Hasan, and L. Pasupulety, "In Situ FTIR Spectroscopic Study of 2-Propanol Adsorptive and Catalytic Interactions on Metal-Modified Aluminas," *Langmuir* 17 (2001): 4025–4034, https://doi.org/10.1021/la001810r.

53. Z. Martinez-Ramirez, S. A. Jimenez-Lam, and J. C. Fierro-Gonzalez, "Infrared Spectroscopic Evidence of Adsorbed Species During the Oxidation of 2-Propanol Catalyzed by γ-Al_2O_3-Supported Gold: Role of Gold as a Hydrogen-Subtractor," *Journal of Molecular Catalysis A: Chemical* 344 (2011): 47–52, https://doi.org/10.1016/j.molcata.2011.05.001.

54. G. A. M. Hussein, N. Sheppard, M. I. Zaki, and R. B. Fahim, "Infrared Spectroscopic Studies of the Reactions of Alcohols Over Group IVB Metal Oxide Catalysts. Part 1.—Propan-2-ol Over TiO_2, ZrO_2 and HfO_2," *Journal of the Chemical Society, Faraday Transactions 1: Physical Chemistry in Condensed Phases* 85 (1989): 1723, https://doi.org/10.1039/f19898501723.

55. M. I. Zaki, G. A. H. Mekhemer, N. E. Fouad, and A. I. M. Rabee, "Structure–Acidity Correlation of Supported Tungsten(VI)-Oxo-Species: FT-IR and TPD Studies of Adsorbed Pyridine and Catalytic Decomposition of 2-Propanol," *Applied Surface Science* 308 (2014): 380–387, https://doi.org/10.1016/j.apsusc.2014.04.180.

56. X. Kang, A. Chatzitakis, T. Aarholt, X. Sun, C. Negri, and T. Norby, "Facet-Engineered TiO_2 Nanomaterials Reveal the Role of Water–Oxide Interactions in Surface Protonic Conduction," *Journal of Materials Chemistry A* 10 (2022): 218–227, https://doi.org/10.1039/D1TA06075A.

57. D. P. Birnie and N. J. Bendzko, "^{1}H and ^{13}C NMR Observation of the Reaction of Acetic Acid With Titanium Isopropoxide," *Materials*

Chemistry and Physics 59 (1999): 26–35, https://doi.org/10.1016/S0254-0584(99)00021-8.

58. W. Sattler and G. Parkin, "Low Temperature NMR Spectroscopic Investigation of a Zinc Bicarbonate Compound: Thermodynamics of Bicarbonate Formation by Insertion of CO_2 Into the Zinc Hydroxide Bond of ZnOH," *Polyhedron* 32 (2012): 41–48, https://doi.org/10.1016/j.poly.2011.08.015.

59. A. Markovits, A. Fahmi, and C. Minot, "A Theoretical Study of CO_2 Adsorption on TiO_2," *Journal of Molecular Structure: THEOCHEM* 371 (1996): 219–235, https://doi.org/10.1016/S0166-1280(96)04696-9.

60. P. Kostestkyy, J. Yu, R. J. Gorte, and G. Mpourmpakis, "Structure–Activity Relationships on Metal-Oxides: Alcohol Dehydration," *Catalysis Science & Technology* 4 (2014): 3861–3869, https://doi.org/10.1039/C4CY00632A.

Supporting Information

Additional supporting information can be found online in the Supporting Information section.

The authors have cited additional references within the Supporting Information.

Supporting File 1: anie73033-supp-0001-SuppMat.docx.